Effect of elastic follow-up and ageing on the creep of an austenitic stainless steel

Y. Q. Wang[1, 2*], H. E. Coules[1], C. E. Truman[1], D. J. Smith[1]

[1] *Department of Mechanical Engineering, University of Bristol, BS8 1TR, UK.*

[2] *United Kingdom Atomic Energy Authority, Culham Science Centre, Abingdon, Oxon. OX14 3DB, UK.*

ABSTRACT

Elastic follow-up is a mechanical boundary condition lying between constant load and constant strain control. It exists in many engineering components operating at high temperature and can result in dramatically different creep stress relaxation and strain accumulation rates in a localized region of a component. We have performed creep tests under constant load, constant strain and elastic follow-up control on an aged (additional 22,000 hours) 316H austenitic stainless steel after service in a nuclear power station for 65,000 hours. Primary and secondary forward creep models with parameters derived from the constant-load data were able to describe constant-load creep adequately, but not able to predict stress relaxation and elastic follow-up. We show that this is because ageing has increased the constant-load creep strain rate significantly but has no effect on stress relaxation creep strain rate. Ageing promotes the formation of ferrite/chi phase at grain boundaries which are preferential sites for creep cavitation under load control. However, creep cavitation is less likely under constant strain and elastic follow-up control because a high creep strain rate, large creep strain and stress cannot coexist under these boundary conditions.

Keywords: Elastic follow-up, ageing, creep stress relaxation, austenitic stainless steel, constitutive equations.

1. INTRODUCTION

The concept of elastic follow-up was initially introduced by Robinson [1] to describe how the creep stress relaxation rate in a bolt was affected by the relative amount of initial elastic deformation in the bolt and bolted flange respectively. This mechanism can be described by a two bar structure which is a specimen linked to a spring in series (Fig. 1a, state 1). The creep specimen acts in the same way as a bolt, and the spring acts the bolted flange. When the whole structure subjected to a fixed displacement (δ_0) a locked-in stress is generated in the specimen and spring, as shown in Fig. 1a state 2. As the stress in the specimen relaxes, due to creep (Fig. 1a state 3), the spring also relaxes. This results in additional displacement and a reduction of the stress relaxation rate in the specimen: a phenomenon known as elastic follow-up. Unlike under constant load or constant strain control, under elastic follow-up both the stress and total strain in the specimen can change.

Elastic follow-up exists in many engineering components operating at high temperature when creeping of a localized region occurs faster than in the surrounding regions [2-4]. In Advanced Gas-cooled Reactors (AGRs), the relaxation of weld-induced residual stress with associated elastic follow-up has contributed to the reheat cracking of welded 316H stainless steel components [2, 5]. During high-temperature service, elastic follow-up reduces the creep stress relaxation rate of material local to the weld and allows creep strain to accumulate here. To extend the lifetime of UK's AGRs elastic follow-up needs to be considered in more accurate

assessments of structural integrity. Therefore, both quantitative determination of the elastic follow-up factor and understanding of its effect on creep deformation are required. The elastic follow-up factor is a scalar that describes the magnitude of elastic follow-up.

The two bar model has been widely used to represent simplified structures such as piping systems [6] and welded components [7], and also to allow determination of the elastic follow-up factor [6-10]. However, there is disagreement about whether elastic follow-up depends solely on the geometry of the structure (and hence its stiffness) or on both the stiffness and on the materials' creep behaviour (creep constitutive equations and constants) [11]. Wang et al. [12] found that when creep only existed in the specimen alone, the remaining bars acting as perfectly elastic elements, the elastic follow-up factor (Z) in a two bar model (Fig. 1a) is given by

$$Z = 1 + 1/\alpha \qquad (1)$$

where α is ratio of the specimen stiffness ($K_1 = A_1 E_1 / L_1$) to the spring stiffness ($K_2 = A_2 E_2 / L_2$). A_1, E_1, L_1 and A_2, E_2, L_2 are cross-sectional area, Young's modulus and length of the specimen and the spring respectively. The stress relaxation rate, creep strain rates and elastic follow-up factor are related in the following way

$$\dot{\sigma}_1 = -\frac{1}{Z} E_1 \dot{\varepsilon}_{1-c} \qquad (2)$$

$$\dot{\varepsilon} = \dot{\varepsilon}_{1-e} + \dot{\varepsilon}_{1-c} = (1 - Z)\frac{\dot{\sigma}_1}{E_1} \qquad (3)$$

where $\dot{\sigma}_1$ is stress relaxation rate in the specimen, $\dot{\varepsilon}_{1-e}$ is the elastic strain rate in the specimen, $\dot{\varepsilon}_{1-c}$ is the creep strain rate in specimen and can be described by a creep equation. The derivation of Eqs. 1 to 3 are detailed in Ref. [12].

The effects of elastic follow-up on creep stress relaxation of SUS 304 stainless steel [1] and aluminium alloy [13], on fatigue cyclic loading of 316FR stainless steel [14], and on crack initiation in 316H stainless steel [15] have been studied using creep testing machines based on the two bar model. The results show that the presence of elastic follow-up reduces the creep stress relaxation rate and introduces additional creep strain into the specimen, and therefore contributes to fatigue damage and crack initiation. Many previous studies have used equation 2 to predict creep stress relaxation [16-19] and elastic follow-up [13] by integration of a forward creep equation, with creep parameters derived using a function fitted to experimental forward creep data. This is because laboratory studies of stress relaxation and elastic follow-up can practically be performed over only a limited number of initial stresses, times and elastic follow-up factors whereas constant load creep data are more widely available. Wang et al. [18] showed that stress relaxation in 316H austenitic stainless steel can be predicted reliably by using an empirical RCC-MR model and constants. However, the case where elastic follow-up is present has not been studied both experimentally and analytically. Since creep is a time-dependent behaviour, the interaction between ageing and boundary conditions makes it unclear whether or not stress relaxation and elastic follow-up can be predicted using a forward creep law and constants based on Eq. 2.

The purpose of the current work is to investigate the feasibility of using creep constitutive models based on constant-load test data to evaluate stress relaxation and elastic follow-up. Constant load, constant strain and elastic follow-up tests were conducted for ex-service laboratory aged (EXLA) 316H austenitic stainless steel. Empirical parameters for the RCC-MR

primary creep and power law creep equations were determined by fitting the equations to the constant load creep data. The RCC-MR primary creep model based on time and strain hardening, and the power law creep model, were then applied to predict the stress relaxation and elastic follow-up. Factors which may affect the predictions include inadequate quantity and scatter of the creep data, limitation of time hardening and strain hardening models, and interaction between ageing and boundary conditions. These factors are discussed in relation to the elastic follow-up test results.

2. MATERIAL, EXPERIMENTS AND RESULTS

2.1. Materials and microstructural characterization

The material in this study was supplied by EDF Energy in an ex-service plus laboratory aged (EXLA) condition. The 316H stainless steel was extracted from steam header HYA 2D1/2 (Cast 69431), that had been in-service at the Heysham nuclear generating station for approximately 65,000 hours in the temperature range of 763K to 803K. This Ex-Service (EX) condition material was then aged isothermally at 823K for 21,000 hours to an "Ex-Service, Laboratory Aged" (EXLA) condition. The chemical composition of the EXLA material is given in Tab. 1 [20]. The scanning electron microscope (SEM) image of Fig. 2a shows the grain structure and cavities of the as-received EXLA material. An electron backscatter diffraction (EBSD) map shows the cavities often associated with ferrite and located at grain boundaries or grain boundary junctions (Fig. 2b).

2.2 Constant load, constant strain and elastic follow-up experiments

Constant load creep tests

A series of uniaxial constant load creep tests were performed by Joseph et al. [21], Chen et al. [20, 22], and the authors. Applied stresses in the range of 126 MPa to 356 MPa at 550 °C were used, as summarised in Tab. 2. All creep tests used lever-type constant load tensile creep machines with constant temperature (variation of less than ±2 °C during holding) using a three-zone resistance furnace. The test specimens were designed to conform to the ASTM E8 [23] and BS EN 10291 [24] standards with a diameter of 5.65 mm and gauge lengths of 28.25 or 35 mm. A pair of Linear Variable Differential Transformers (LVDTs) with a displacement resolution of approximately 1 μm were used to monitor the development of total strain in each specimen, and three thermocouples (Type K) were attached to the top, middle and bottom of the specimen gauge length. Each specimen was heated to 550 °C after which a known tensile load (recorded by a load cell) was applied.

Elastic follow-up tests

Since it is difficult to perfectly constrain a two bar experimental setup (Fig. 1a), we developed a three bar rig (Fig. 1b) [25] for performing elastic follow-up experiments. As with the two bar model, a locked-in stress in a specimen can be generated through strain incompatibility in the three bar model, as shown in state 2 in Fig. 1b. In state 3, the specimen can creep at high temperature while the remaining parts of the system are purely elastic elements at room temperature. The relative stiffness of the spring and the creeping sample dictates the values of Z, which are given by;

$$Z = 1 + 1/\beta + 1/\gamma \quad (4)$$

where β and γ are the stiffness ratios between the specimen and the remaining elements of system, bars 2 and 3. The stiffness ratios are given by

$$\beta = K_2/K_1, \gamma = 2K_3/K_1 \quad (5)$$

where K_1, K_2 and K_3 are the stiffnesses of the specimen, bars 2 and 3 given by

$$K_1 = A_1E_1/L_1, K_2 = A_2E_2/L_2, K_3 = A_3E_3/L_3 \quad (6)$$

A E and L are the cross section, Young's modulus and bar length for each element respectively. The derivation of Eq. 4 is detailed in Appendix A.

Eq. 4 shows that if bars 2 and/or 3 are very compliant (β <<1 and/or γ <<1), Z becomes infinitely large ($Z \to \infty$) which approximates a constant load applied to the specimen. By contrast, if bars 2 and 3 are very stiff (β >>1 and γ >>1), the elastic follow-up factor is Z : 1, approximating displacement-controlled conditions.

Three test machines were designed based on the three bar system with a specimen, an elastic bar and a load cell connected in series [26]. This series system was then linked to outer parallel bars. By changing the sizes of the elastic elements (Bar 2) or the specimen, a range of elastic follow-up factors (about Z = 1.2, 5 and 20) was obtained. Rig 1 was designed to produce elastic follow-up factors of 4.8 and 20. Part of the elastic follow-up factor in Rig 1 is introduced by Bars 3 which the total stiffness is approximately 25 kN/mm. The frames of Rig 2 and Rig 3 were very rigid (i.e. the stiffness of bars 2 and 3 are large), and therefore these rigs could produce a small elastic follow-up factor (~ 1.2) when using a specimen 6 mm in diameter and 150 mm in length. Rig 2 and Rig 3 also enabled the connection of a short specimen to a removable aluminium

elastic bar (bar 2) to obtain follow-up factor as large as 20.

Nine high-temperature elastic follow-up tests were conducted. The specimen dimensions, rig used, intended elastic follow-up factor and applied initial stress are summarized in Tab. 3. The test procedure for the elastic follow-up test was the same as for the constant-load creep test until the application of tensile load. However, for the elastic follow-up tests, a tensile displacement was applied using a loading screw. The average strain rate during loading was approximately 4 x 10^{-5} s^{-1}. Loading-up was stopped when the stress in the specimen reached the target value. In the elastic follow-up tests, the stress subsequently decreased over time due to creep relaxation.

Constant strain test

One constant strain (Z=1.2) test with an initial applied engineering stress of 250 MPa at 550 °C was conducted using a Mayes 20 kN servo-electric creep test machine. Results from this test were compared to the elastic follow-up tests with Z=1.2 using rigs 2 and 3, in order to verify that the same constant strain control was achieved using mechanical control as when using servo-electric control.

A specimen with a diameter of 8.48 mm and gauge length of 60 mm was used, and its extension was measured by a pair of capacitance extensometers with a maximum extension of 2 mm. Three Type N thermocouples were used to measure the temperature profile along the gauge length of the specimen. The temperature on specimen was maintained to within ±0.5 °C at 550 °C during the test. The specimen was loaded to 250 MPa at a strain rate of 6.7 x 10^{-5} s^{-1} under load control. Once the stress was at 250 MPa, displacement control was activated to keep the strain in the

gauge length of specimen constant as the stress relaxed due to creep. This test was continued for 1050 hours.

2.3 Constant load, constant strain and elastic follow-up experiment results

The results of constant load creep tests are shown in Fig. 3 for a range of stresses. The secondary creep strain rates with respect to applied true stress are shown in Fig. 4 for all of the tests. The secondary creep strain rate increases with increased applied stress.

The elastic follow-up experimental results are shown in Figs. 5 and 6. The specimens were loaded to different initial stresses of approximately 350 MPa, 250 MPa and 235 MPa and then allowed to relax with different elastic follow-up factors: 1.2, 4.7 and 21. Overall, Figs. 5 and 6 show that the presence of elastic follow-up decreases the rate of stress relaxation and introduces additional creep strain accumulation. Figs. 5a, 5c and 5e show that the stress-strain trajectories for different levels of elastic follow-up and initial stress are approximately linear. This indicates that the elastic follow-up factor was approximately constant during stress relaxation. The intended elastic follow-up factors agreed closely with the measured elastic follow-up factors, as summarized in Tab. 3. In addition, the response of bar 2 was purely elastic during both loading up and stress relaxation stages. This provides confidence that the rigs produce constant elastic follow-up factors at the intended magnitude. Figs. 5b, 5d and 5f show the corresponding stress relaxation for the full range of different applied stresses and elastic follow-up factors. Fig. 6 shows that irrespective of the level of elastic follow-up there is an initial rapid reduction in the stress, but although this reduction is substantial when Z~1 it is smaller for high values of Z.

The creep stress relaxation curves from servo-electric and mechanical rigs are compared in Fig. 6b. The data measured using the newly-designed creep machine agreed well with creep data measured using the servo-electric machine.

2.4 Comparison of constant load and constant strain results for EX and EXLA material

The results of constant-load and constant-strain creep tests for material in the EXLA condition were compared to results for material in the EX condition [18] to determine the effect of ageing on creep deformation. The 22,000 h post-service heat treatment at 550 °C decreased the material's resistance to plastic deformation during loading and accelerated the constant load creep strain rate significantly (Fig. 4). Also, the true creep strain at failure increased from around 5-16% in EX material to approximately 30 % in EXLA material. Although the ageing has a significant effect on constant load creep tests, Fig. 8 shows that the ageing has no effect on creep stress relaxation tests since the creep stress relaxation curves in EX and EXLA materials agree closely.

3. PREDICTION OF STRESS RELAXATION WITH ELASTIC FOLLOW-UP

3.1 Elastic follow-up prediction models

We selected the RCC-MR primary and power law creep models [3] to predict elastic follow-up behaviour since they are used routinely to assess the structural integrity of stainless steel components operating at high temperature. The parameters in these models are normally derived

using data obtained from constant-load creep tests.

The RCC-MR model assumes that the creep curve is described by

$$\varepsilon_c = \varepsilon_{pc} + \varepsilon_{sc} = \varepsilon_{pc} + \dot{\varepsilon}_{sc}(t - t_p) \quad (7)$$

where ε_c is total creep strain at total time t (in hours). ε_{pc} is primary creep strain at primary creep time (t_P in hours). ε_{sc} and $\dot{\varepsilon}_{sc}$ are secondary creep strain and secondary creep strain rate respectively. The equations for creep strain, according to [3] are:

$$\varepsilon_{pc} = C_1 t^{C_2} \sigma^{n_1}, \text{ For } 425°C \le \theta \le 700°C \text{ and } t \le t_P \quad (8)$$

$$\varepsilon_c = C_1 t_p^{\,C_2} \sigma^{n_1} + C\sigma^n (t - t_P), \text{ For } 480°C \le \theta \le 700°C \text{ and } t > t_P \quad (9)$$

where σ is the applied stress in MPa at time t and C, C_1, C_2, n and n_1 are the material constants, which are functions of the temperature T. The transition from primary to secondary creep is given by the condition

for 425°C < θ ≤ 480°C, $t_P = \infty$ (10)

for 480°C < θ ≤ 700°C, $t_P = C_3 \sigma^{n_3}$ (11)

where $C_3 = \left(\frac{C}{C_1 C_2}\right)^{\frac{1}{(C_2 - 1)}}$ and $n_3 = \frac{(n - n_1)}{(C_2 - 1)}$ (12)

Eq. 11 shows that the primary creep time increases with decreases of the applied stress. Hence, the primary creep time is infinitely large for stress relaxation tests [18]. In the present work, the primary part of RCC-MR (Eq. 9) is adequate to describe primary and secondary creep stages. Therefore, we do not have to separate the primary and secondary stage in constant load tests as well as in stress relaxation tests.

The prediction of stress relaxation as well as elastic follow-up can be performed through integration of Eq. 2 based on the RCC-MR primary creep equation given by

$$\varepsilon_c = C_1 t^{C_2} \sigma^{n_1} \qquad 13$$

A time hardening (TH) solution based on Eq. 13 is given by:

$$\dot{\varepsilon}_c = C_2\, C_1 t^{C_2 - 1} \sigma^{n_1} \qquad \textit{Time hardening} \qquad 14$$

and from Eq. 14, we get:

$$t = \left(\frac{\varepsilon_c}{C_1 \sigma^{n_1}} \right)^{\frac{1}{C_2}} \qquad 15$$

Alternatively, by substituting Eq. 15 into 14, we obtain a strain hardening (SH) solution given by:

$$\dot{\varepsilon}_c = C_2\, C_1^{\frac{1}{C_2}} \sigma^{\frac{n_1}{C_2}} \varepsilon_c^{\frac{C_2 - 1}{C_2}} \qquad \textit{Strain hardening} \qquad 16$$

It is important to note that the strain and time hardening analyses predict same creep strain rates during steady state creep.

In constant-strain and elastic follow-up creep tests, the elastic strain is replaced by creep strain as creep deformation occurs. The creep strain is given by

$$\varepsilon_c = \mathrm{Z} \cdot \frac{\sigma_0 - \sigma}{E} \qquad 17$$

where σ_0 and σ are initial and current applied stress respectively.

Substituting Eqs. 14, 16 and 17 into Eq. 2, we obtain a time hardening and strain hardening solutions for the rates of stress relaxation with elastic follow-up

$$d\sigma/dt = -\frac{1}{Z} EC_1 C_2 t_P^{\,C_2-1} \sigma^{n_1} \qquad \textit{Time hardening} \qquad (18)$$

$$d\sigma/dt = -\frac{1}{Z} (EC_1)^{1/C_2} C_2 \left[Z(\sigma_0 - \sigma) \right]^{(C_2-1)/C_2} \sigma^{n_1/C_2} \qquad \textit{Strain hardening} \qquad (19)$$

The strain hardening model considers the accumulated creep strain in the specimen due to the elastic follow-up which further decreases the creep stress relaxation rate.

A power-law creep model was also applied to predict stress relaxation. This may be expected to provide a lower-bound estimate of the creep strain rate, since the material constants are derived from the secondary creep deformation rate only.

$$\dot{\varepsilon}_{sc} = C\sigma^n \qquad (20)$$

where C and n are material constants. By substituting Eq. 20 into 2, we obtain a solution for stress relaxation with elastic follow-up based on secondary creep alone:

$$\sigma = \left[(n-1)\frac{1}{Z} ECt + \sigma_0^{\,1-n} \right]^{1/1-n} \qquad (21)$$

In this paper, Eqs. 18, 19 and 21 are used to predict the material behaviour during stress relaxation with different values of elastic follow-up factor. The results of the constant load creep tests described in Section 2.2 were used to obtain the creep constants for Eqs. 13 and 20.

3.2. Model constants fitting

Durations of the primary and secondary creep stages for all stress levels were obtained from experimental creep data. The constants in Eq. 13 were determined by taking logs and performing linear regression:

$$In\left(\varepsilon_{pc}\right) = In\left(C_1\right) + C_2 In\left(t_p\right) + n_1 In\left(\sigma\right) = H + C_2 In\left(t_p\right) + n_1 In\left(\sigma\right) \quad (22)$$

where $C_1 = e^H$ (23)

For the current work we retained the value of n_1 given in the conventional RCC-MR data, and then used Eq. 22 to determine the new constants H and C_2 for each test.

Previous work [3] assumed that the parameters C_1 and C_2 were material constants which depend on temperature alone and were independent of the stress level. However, Fig. 7 shows that at 550°C C_2 is significantly dependent on the applied stress while the constant H is weakly dependent. Therefore, to provide an improved fit to the experimental data we assumed that H and C_2 are linearly dependent on stress:

$$H \pm \delta H = a\sigma + (b \pm \delta b) \quad (24)$$

$$C_2 \pm \delta C_2 = c\sigma + (d \pm \delta d) \quad (25)$$

where a, b, c and d are material constants. The errors on $H(\delta \mathrm{H})$ and $C_2(\delta C_2)$ were obtained from errors on $b\left(\delta b\right)$ and $d\left(\delta d\right)$. The two linear Eqs. 24 and 25 were used to fit the constants a, b, c and d, making values of H and C_2 dependent on the applied stress. The upper (δH and δC_2) and lower ($-\delta H$ and $-\delta C_2$) bound curves of H and C_2 correspond to offsetting the mean line by $\pm\delta b$ and $\pm\delta d$, assuming that the slopes (values of a and c) are constant [27]. The fitted curves for H and C_2 are shown in Fig. 6 and a set of coefficients (a, b, $\pm\delta b$, c, d and $\pm\delta d$) are given in Tab. 4.

Secondary (or steady-state) creep strain rate data for each test are shown in Fig. 4. The material constants C and n were obtained by using linear regression:

$$In(\dot{\varepsilon}_{sc}) = InC + nIn\sigma \qquad 26$$

Figure 3 shows that the variation is generally log-linear over the range of data available and that such a power law equation describes the behaviour adequately. The resulting constants for the paw law creep Eq. 26 are summarized in Tab. 4.

Curves of creep strain as a function of time, created by using Eq. 13 together with newly derived material constants, are shown in Fig. 3 together with experimental results for six constant load creep tests. Compared with conventional RCC-MR constants and ex-service (EX) constants, the newly fitted (EXLA) constants provide improved predictions for constant load creep with applied true stresses in the range 125 to 356 MPa.

3.3. Prediction results

Predictions of elastic follow-up were made using Eqs. 18, 19 and 21 together with the newly-derived EXLA material constants given in Table 4. The equations were solved using the Matlab ode45 ordinary differential equation solver [28]. The prediction for each test using power law, RCC-MR primary time hardening and strain hardening models are shown in Figs. 9 a-c, d-f and g-i respectively. The power law underestimates the initial stress relaxation rate but overestimates the stress relaxation after 1-1000 hours, depending on the initial applied stress. Both the RCC-MR primary time hardening and strain hardening equations overestimate the level of stress relaxation for almost all of the tests and durations.

Predictions for all tests are also illustrated in Fig. 10, which compares predicted stress with the observed stress. The figure shows bounds on the predictions, with positive and negative values representing an overestimate and an underestimate of predicted stress relaxation. The predictions using the power law lie between error bounds of approximately -25 MPa to 50 MPa (Fig. 10a). The Time Hardening (TH) and Strain Hardening (SH) equations predict very similar specimen responses. The predictions using RCC-MR primary TH model lie between error bounds of about 0 MPa and 95 MPa, but the error narrowed to between 5 MPa and about 55 MPa for longer durations (Fig. 9b). Compared to TH model the error bounds when using SH model are shifted down, becoming -10 MPa to 80 MPa (Fig. 10c).

RCC-MR primary TH and SH models with EX creep constants [18] (Tab. 2) were also used to predict the stress relaxation and elastic follow-up behaviour for EXLA samples. The results are shown in Fig. 11. It shows that the predictions using the RCC-MR primary TH model have error bounds of about -10 MPa and 35 MPa, but the error shifted to between -20 MPa and 25 MPa when using the SH model. Compared to EXLA constant, the using of EX constants improved the prediction in all cases. Therefore, the forward creep properties of material in the EX condition can satisfactorily predict the relaxation of material in the EXLA condition using the empirical RCC-MR model.

4. DISCUSSION

4.1. The effect of elastic follow-up on macroscopic stress relaxation

The effect of elastic follow-up on creep stress relaxation is directly proportional to the initial applied stress and elastic follow-up factors, and inversely proportional to the creep-resistance of the material. When the elastic follow-up factor is close to 1 (i.e. fixed-displacement conditions) the stress tends to converge after 1000 to 10000 hours of creep (Fig. 5a). Figs. 5b, 5d and 5f show that the rate of convergence decreases significantly with increasing elastic follow-up factor. For initial stresses of 235 MPa, 255 MPa and 355 MPa, the difference in remaining stress after 1000 hours for specimens with Z=1.2 and 21 were approximately 60 MPa, 70 MPa and 90 MPa respectively (see Fig. 6). Hence, the presence of elastic follow-up increases the convergence time significantly.

In this study, creep properties were determined from accelerated (i.e. high stress) tests and may not be applicable to long-term low stress behaviour of the actual high temperature components in nuclear power plants. For a 316H austenitic stainless steel component at 550°C, the effect of elastic follow-up on creep will be small if the stress in the component is less than 100 MPa because the stress relaxation rate is extremely low. The stress fields in nuclear power plant components are generally complex and multiaxial: thermal, residual and externally-applied stresses often occur together. Although welding residual stresses in non-stress-relieved austenitic steel welds can be large (up to 350 MPa [29]), welded components with low elastic follow-up factors accumulate far less creep deformation than a component under an equivalent applied load. However, the accumulation of creep strain in a localized region can exacerbate problems of creep crack initiation. Furthermore, the presence of of elastic follow-up during the dwell of a creep-fatigue cycle increase creep strain accumulation [14]. Therefore, the consideration of elastic follow-up in the integrity assessment of AGRs is dependent on the specific creep problem

and structure, and factors that can affect the creep deformation, such as plasticity [30], operating conditions, and thermal gradients must be considered during analysis.

4.2 Prediction of stress relaxation in elastic follow-up conditions

In the present study, the RCC-MR primary creep and power creep laws together with newly-derived constants for EXLA material were used to predict stress relaxation and elastic follow-up based on Eq. 2. The EXLA constants provide a good prediction for forward creep, but not for stress relaxation and elastic follow-up.

An inadequate quantity of constant load-creep data, and scatter in the data, could negatively affect the results of predictions based on modelling constants derived from these data [18]. In the present study, the range of stresses (130-350 MPa) used in the stress relaxation and elastic follow-up tests was within the stress range used for constant load creep tests. As shown in Fig. 3c the EXLA constants are adequate to predict the forward creep deformation. Therefore, constants obtained from constant load creep data were sufficient to predict creep deformation under constant strain and elastic follow-up control. The scatter of creep strain can be observed by replicate tests at the same temperature and load [31]. There were fourteen constant load creep tests (LC8-11 and LC14-23) conducted with an applied engineering stress of 250 MPa at 550 °C, as summarised in Table 2. The creep strain rate and accumulated creep strain can vary by a factor of two for identical conditions (Fig. 4). Upper bound, mean and lower bound constants were derived to consider the effect of scatter, however, these differing constants were found to have little effect on stress relaxation predictions. Figure 6b shows four creep stress relaxation tests for EXLA samples with applied engineering stress of 250 MPa at 550°C. The discrepancies in the short and long term were

as small as 10 MPa. This indicates that the scatter of the stress relaxation data was small. Elastic follow-up tests with the same elastic follow-up factors but different applied stresses, or the same initial applied stresses but different elastic follow-up factors, agreed with each other – further demonstrating that the scatter in the elastic follow-up test results was small. Therefore, the inaccuracy of the predictions is not caused by insufficient constant-load creep data or scatter of data.

Forward creep models are often applied to predict stress relaxation and elastic follow-up based on time hardening or strain hardening. Consequently, the forward creep models and constants cannot predict stress relaxation and elastic follow-up if the internal state of the material is not a function of creep time or strain only. For example, in 316H austenitic stainless steel at 550 °C creep deformation mainly results from dislocation glide and climb [32]. Resistance from precipitate particles and solute atoms gathering around active dislocation sites need to be overcome during creep. Under isothermal conditions, precipitate nucleation, growth and coarsening (size, volume fraction and number density) are affected by the interaction of the applied stress, time and strain [33]. Therefore, the time- and strain-hardening models cannot accurately reflect the effect of precipitate strengthening in an isothermal creep test as they cannot consider the effect of the currently applied stress. As a result, Eq. 2 cannot predict the stress relaxation and elastic follow-up behaviour precisely if precipitate nucleation and coarsening are significant during creep. In the present study, 316H in the EXLA condition is a long-term-aged material: i.e. further precipitation strengthening should not occur during the relatively short period of creep time at 550°C. The reduction in athermal solute strengthening due to the depletion of solute atoms by precipitation should also be negligible [34].

The third possible reason for the poor performance of the EXLA constants in predicting stress relaxation is the effect of boundary conditions on the evolution of intergranular stress between different grain families. The intergranular stress in a bulk polycrystalline material can be created during loading to above the yield stress due to elastic-plastic anisotropy at the length-scale of grains [35-39]. Creep can also generate intergranular stress in Type 316H austenitic stainless steel when a greater degree of (time-dependent) deformation occurs in preferentially-oriented crystallites [22, 40]. Intergranular stress can change the internal resistance and effective stress in materials, changing the macrocopic material properties [18, 20, 41-43]. However, it is not clear how the intergranular stress evolves during stress relaxation. Recently, Wang et al., [44, 45] showed that in 316H in the EXLA condition, the intergranular stresses between different grain families remained constant during forward creep, stress relaxation and elastic follow-up tests. Therefore, the ratio of intergranular stress to the current applied stress increases during stress relaxation and elastic follow-up tests while remaining constant during forward creep tests. Nevertheless, the intergranular stress does not affect the creep deformation since the creep strain decreased significantly during the primary stage of a constant-load creep test while intergranular stress was constant [44]. Therefore, the difference of the intergranular stress under different boundary conditions is also not the reason of inaccuracy of the EXLA model predictions.

Fig. 3 shows that the effect of ageing on accumulated forward creep strain increases with greater applied stress. This is also reflected in Fig. 9 which shows that for higher initial stresses, there is a greater discrepancy between observed and predicted stress during relaxation. However, when the applied stresses relaxed to a certain value (200 MPa to 270 MPa), the discrepancies

decreased. This is because the effect of ageing on accumulated creep strain is small, and the stress relaxation tests tend to converge to each other in the long term irrespective of elastic follow-up, initial stress and material's properties.

Although the forward creep properties of the EXLA and EX materials are different (Fig. 3 and 4), the stress relaxation behaviour was found to be similar (Fig. 8). This demonstrates that although ageing has a significant effect on the materials' forward creep properties, it does not change their stress relaxation and elastic follow-up behaviour. The successful prediction of stress relaxation and elastic follow-up behaviour of EXLA material using EX condition forward creep constants confirms this finding. The possibility that the effects of ageing could interact with mechanical boundary conditions, affecting the creep deformation rate, is discussed in the next section.

4.3 Effect of ageing and mechanical boundary conditions on creep deformation

The detrimental influence of extended ageing of 316H steel at high temperatures on its creep resistance has, in part, been attributed to the recovery of the dislocation structure, coarsening of $M_{23}C_6$ precipitates and formation of secondary phases including ferrite, sigma, chi and G-phase [46-50]. Warren et al., [47] showed that 316H in the EX condition contains approximately 0.16vol% ferrite. Furthermore, more than half of analysed cavities were observed to nucleate and grow preferentially at the austenite-austenite-ferrite boundary junctions. Warren et al., [47] further characterised the materials in EXLA condition and found that the additional 22,000 h of ageing led to the formation of additional approximately 1.8vol% ferrite. Most recently, Martinez-Ubeda et al., [48] demonstrated that part of the ferrite could, in fact, be chi-phase.

Dyson [51] indicated that the creep cavity number density (N_a) is a function of the density of grain boundary precipitates (N_p) which is given by

$$N_a = fN_p\left(1-\exp^{-k\varepsilon}\right) \quad 27$$

where f is function of interfacial energy (γ) and local tensile stress normal to the grain boundary (σ). K is a measure of the cavity interaction and ε is the strain. Therefore, the ageing introduced significant numbers of second phase particles (ferrite/Chi) at grain edges and corners which offer energetically favourable boundaries predisposed to cavity nucleation and growth (Eq. 27).

The value of critical stress (σ_{crit}) required to ensure a stable creep cavity can be described by

$$\sigma_{crit} = 2\gamma / r_{crit} \quad 28$$

The critical stress is a local stress normal to the grain boundary. This local stress can be partly contributed by the lattice mismatch between austenite-chi phase or austenite-ferrite unit cell. Grain boundary sliding can produce a stress concentration at the particle-matrix interface. This stress is much higher than the applied stress and thus decreases the incubation time for nucleation by several orders of magnitude. During creep at elevated temperature, the stress concentration around the particle-matrix interface generated during loading-up can be relaxed since the elastic deformation is accompanied by creep plasticity and/or diffusional flow [52-54]. However, the evolution of the stress concentration in creep tests under constant load, constant strain and elastic follow-up control might be different.

In addition, a creep damage model proposed by Yin and Faulkner [55] shows that the creep damage parameter is a function of stress, strain and strain rate. Overall, an important deduction from many researchers was that the creep strain, creep strain rate, applied stress and stress concentration are closely associated with cavity nucleation and growth [51, 52, 56, 57]. The majority of previous studies have focused on crack or cavity nucleation or growth under load control, but not under constant strain or elastic follow-up control. The major difference between creep under constant-load and stress relaxation conditions is that under stress relaxation (and elastic follow-up with relatively low Z) high applied stress, large creep strain and creep strain rate cannot coexist. This is firstly because under stress relaxation and elastic follow-up conditions, the total strain is limited. Secondly, the creep strain (ε), creep strain rate ($\dot{\varepsilon}$) and current applied stress (σ) follow $\sigma = \sigma_0 - \frac{1}{Z} E\varepsilon$ and $\dot{\sigma} = -\frac{1}{Z} E\dot{\varepsilon}$, where σ_0 is the initial applied stress. Consequently, sufficient creep strain accumulation to produce significant cavity nucleation and growth is not possible under stress relaxation or low elastic follow-up conditions.

5 CONCLUSION

This study has investigated the effect of mechanical boundary conditions and ageing on creep deformation of Type 316H austenitic stainless steel, and has demonstrated that:

- During stress relaxation at high-temperature, the presence of elastic follow-up decreases the stress relaxation rate and increases the total creep deformation that accumulates in the long-term. This effect is directly proportional to the initial applied stress and elastic follow-up factor. It is inversely proportional to the creep-resistance of the material.

- Creep constants for aged 316H accurately describe this material's behaviour during forward creep, but not under stress relaxation or elastic follow-up conditions. Under these conditions, using creep constants for un-aged 316H consistently produced better predictions of the stress relaxation rate. This suggests that mechanical boundary conditions applied during high-temperature deformation can interact with the material's internal state.
- Ageing promotes the formation of ferrite/chi phase particles at grain boundaries. These are preferential sites for generating the stress concentration required for creep cavity nucleation and growth under load control but not under constant strain and elastic follow-up control (depending on the value of the elastic follow-up factor). Therefore, care needs to be taken when using forward creep models to predict stress relaxation and elastic follow-up. A model which considers the material's internal state is needed to estimate creep properties under different mechanical boundary conditions, creep times and temperatures.

ACKNOWLEDGEMENTS

This paper is dedicated to the memory of David Smith (1951-2015), Professor of Engineering Materials at University of Bristol. He was a charismatic and well-respected member of the Department with limitless enthusiasm for this subject. The authors thank EDF Energy for funding this work. This paper is published with their permission. Yiqiang Wang thanks Mike Spindler and David McLennon for their help with stress relaxation tests at EDF Energy's materials testing laboratory.

Tables

Table 1. Chemical composition (wt.%) of ex-service Type 316H stainless steel [20].

C	Si	Mn	P	S	Cr	Mo	Ni	Co	B	Fe
0.06	0.4	1.98	0.021	0.014	17.17	2.19	11.83	0.10	0.005	Bal.

Table 2. Experimental parameters and results for ex-service laboratory aged samples (EXLA) from HYA 2D1/2 (cast 69431) tested at 550°C at engineering stresses of 320, 300, 280, 260, 250, 185 and 125 MPa. Tests LC1-LC9, LC10-13 and LC14-23 conducted by Joseph et al. [21], the authors and Chen et al. [20, 22, 58, 59] respectively.

Test ID	Engineering /True stress (MPa)	Test duration (hours)	True total creep strain (%)	H	C2	Min creep strain rate h^{-1}%
LC 1	320/354	256.5	25.71	-30.64	0.766	$6.67\cdot10^{-2}$
LC 2	320/356	156.1	28.42	-30.20	0.757	$1.15\cdot10^{-1}$
LC 3	300/329	627.4	19.95	-30.86	0.716	$2.02\cdot10^{-2}$
LC 4	300/326	570.5	28.55	-31.20	0.804	$2.77\cdot10^{-2}$
LC 5	300/331	380.9	31.76	-30.25	0.681	$4.78\cdot10^{-2}$
LC 6	280/304	934.7	27.17	-30.84	0.738	$1.82\cdot10^{-2}$
LC 7	260/279	2350.8	35.42	-30.46	0.619	$7.99\cdot10^{-3}$
LC 8	250/267	4059.4	30.14	-30.66	0.629	$4.29\cdot10^{-3}$
LC 9	250/266	3023.2	21.78	-30.03	0.549	$4.90\cdot10^{-3}$
LC 10	250/260	1145	5.7	-30.42	0.599	$4.06\cdot10^{-3}$
LC 11	250/258	1030	3.88	-30.22	0.533	$2.76\cdot10^{-3}$
	125/125	1174	0.0065	/	/	$7.16\cdot10^{-6}$
LC 12	185/186	1718	0.515	-29.71	0.344	$1.45\cdot10^{-4}$
LC13	152/153	1200	0.093	-4.47	0.281	$2.40\cdot10^{-5}$
LC 14	125/125	2677	0.018	-29.95	0.137	$2.62\cdot10^{-6}$
LC 15	250/257	/	/	-30.98	0.621	$3.42\cdot10^{-3}$
LC 16	250/258	/	/	-30.25	0.512	$4.04\cdot10^{-3}$
LC 17	250/262	/	/	-29.82	0.513	$5.90\cdot10^{-3}$
LC 18	250/262	/	/	-29.77	0.503	$4.57\cdot10^{-3}$
LC 19	250/261	/	/	-29.78	0.487	$3.67\cdot10^{-3}$
LC 20	250/265	/	/	-29.65	0.509	$6.00\cdot10^{-3}$
LC 21	250/261	/	/	-30.04	0.549	$4.65\cdot10^{-3}$

LC 22	250/261	/	/	-29.92	0.527	$4.60 \cdot 10^{-3}$
LC 23	250/265	/	/	-29.65	0.485	$5.61 \cdot 10^{-3}$
LC 24	250/264	/	/	-30.031	0.541	$4.63 \cdot 10^{-3}$

Table 3. Summary of creep stress relaxation and elastic follow-up tests for Type 316 H stainless steel at 550°C with designed elastic follow-up factors 1, 1.2, 4.5, 20 and applied initial engineering stress 205, 230, 250 and 325 MPa. SCM indicates Servo-Controlled Machine.

Test ID	Test Rig	Sample diameter/length (mm)	Initial applied Engineering/true stress (MPa)	Loading up elastic-plastic strain, %	Test duration (h)	Final true stress (MPa)	Designed/ measured Z
EFU 1	3	4.04/70.56	326/357	9.67	860	181	1.2/1.6
EFU 2	3	6.07/70.76	328.5/349	6.19	703	222.5	4.5/4.7
EFU 3	1	7.01/31.2	329/351	6.6	1030	254	20/22.5
CS1	SCM	8.481/60	250/253.5	1.4	1050	139.5	1/1
EFU 4	2	6.05/150.7	249/255	2.69	1132	148	1.2/1.5
EFU 5	2	6.03/150.9	255.5/264	3.42	17	215.5	1.2/1.4
EFU 6	1	7.01/31.2	248/254	2.38	2092	213	20/21.5
EFU 7	2	6.06/151.1	231/235	1.86	2613	125	1.2/1.2
EFU 8	1	6.01/151.4	230.5/233	1.14	1795	162.8	4.5/4.7
EFU 9	1	7.07/30.4	230.5/233	0.934	1918	192.5	20/23
EFU 10	1	6.03/151.2	207/208	0.52	2162	157	4.5/5

Table 4. EXLA, EX and conventional RCC-MR creep constants described using a linear function with applied stress for the primary components. The creep strain is dimensionless; stress is given in MPa, and time in hours. CONV means conventional.

Constants	a	$b \pm \delta b$	c	$d \pm \delta d$	n_1	A	n
EXLA	-0.0037	-29.24 ± 0.33	0.0027	-0.163 ± 0.04	4.18	$1.29 \cdot 10^{-28}$	9.72
EX [18]	-0.0046	$-30.68^{+1.44}_{-1.22}$	0.0026	$-0.064^{+0.15}_{-0.2}$	4.18		
CONV [3]	0	-31.15	0	0.421	4.18		

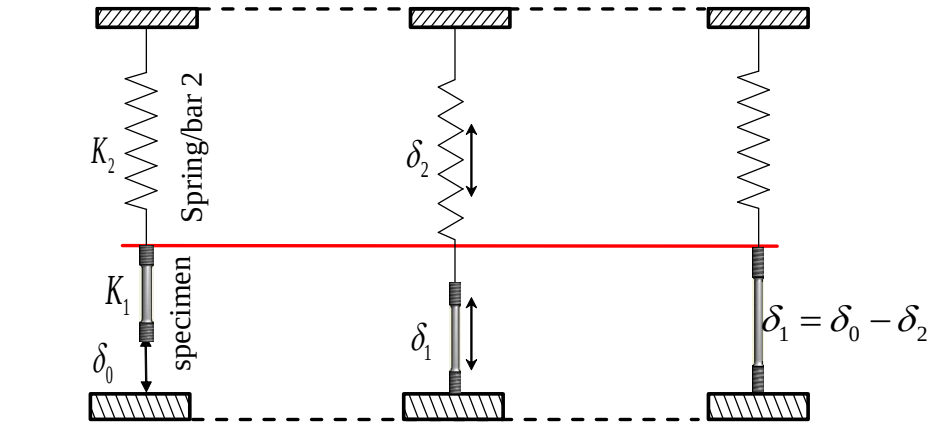

State 1: Initial misfit State 2: Locked-in stress State 3: Creep

(a) Two bar model

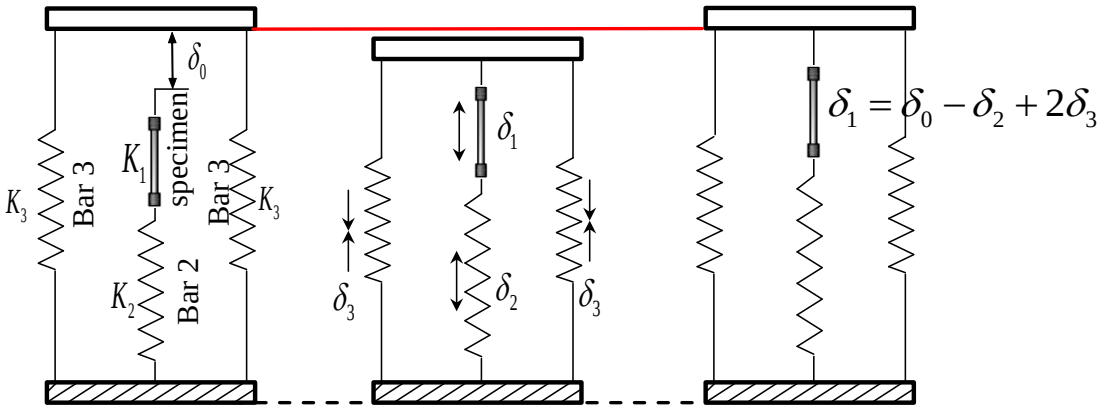

State 1: Initial misfit State 2: Locked-in stress State 3: Creep

(b) Three bar model

Figure 1. Schematic diagrams illustrating (a) a two bar model and (b) a three bar system which both could produce elastic follow-up in a test specimen during creep stress relaxation. A locked-in tensile stress can be generated in the specimen (state 2) by the introduction of a misfit shown in state 1.

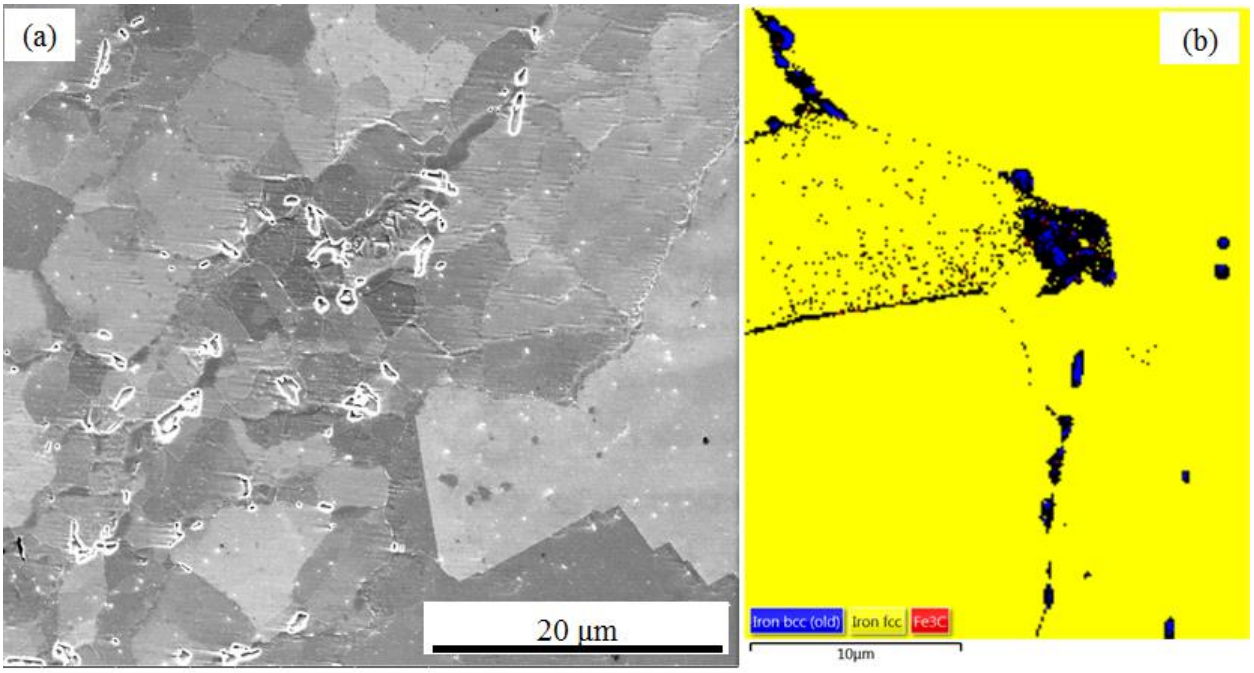

Figure 2. (a) SEM image of the as-received EXLA material showing cavities at the grain boundaries and triple joints (b) the corresponding EBSD map for a small region showing the phase distribution. Yellow grains are austenite, blue grains are ferrite.

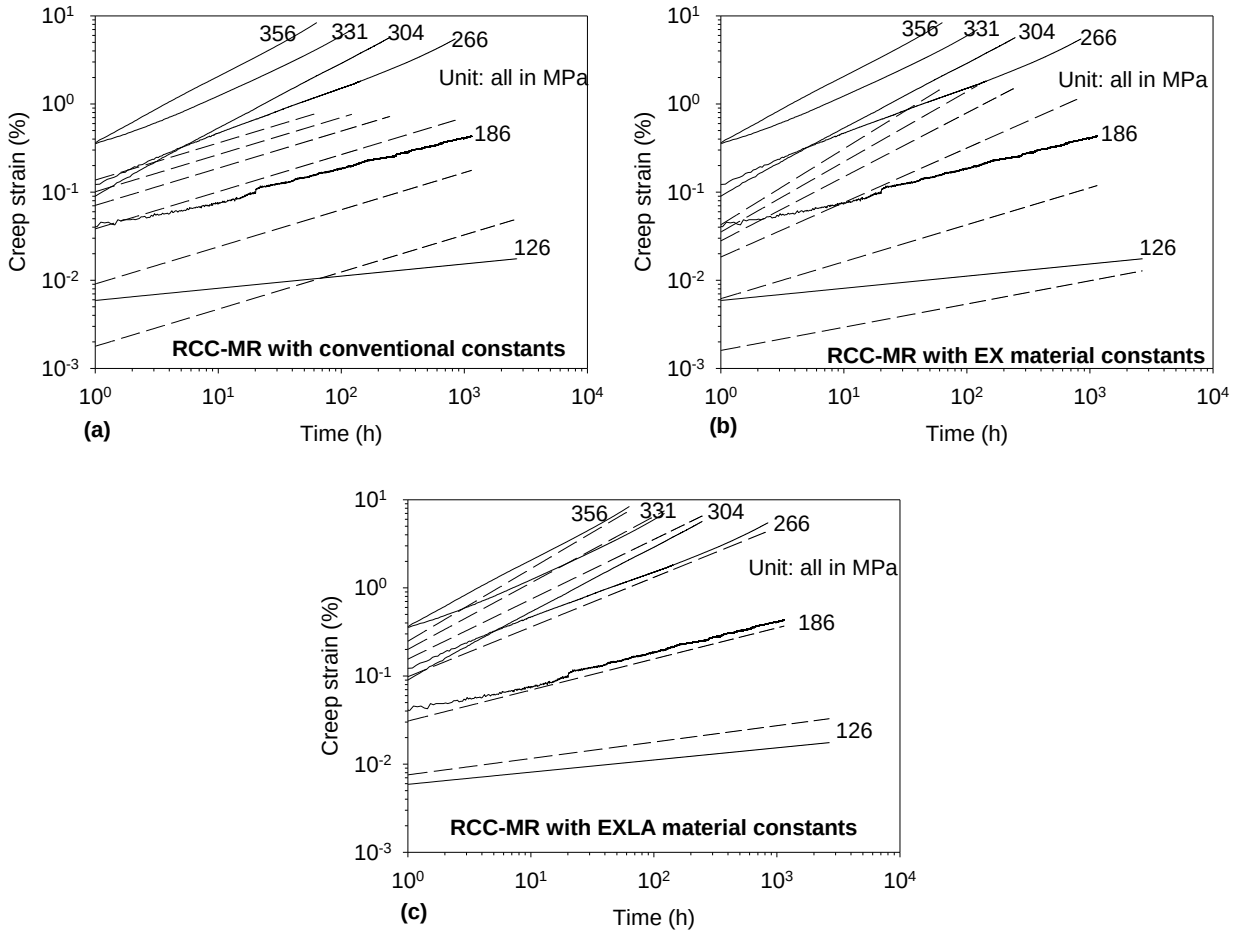

Figure 3. Creep strain versus time for Type 316H stainless steel in ex-service laboratory aged (EXLA) condition with constant applied stress from around 120 to 360 MPa at 550 °C (solid lines in Figs. 3a, b and c). Simulated creep curves using an RCC-MR model with conventional, EX and EXLA material constants also shown in Fig. 3(a), 3 (b) and 3(c) respectively (dash lines). EX represents ex-service and EXLA represents ex-service laboratory aged.

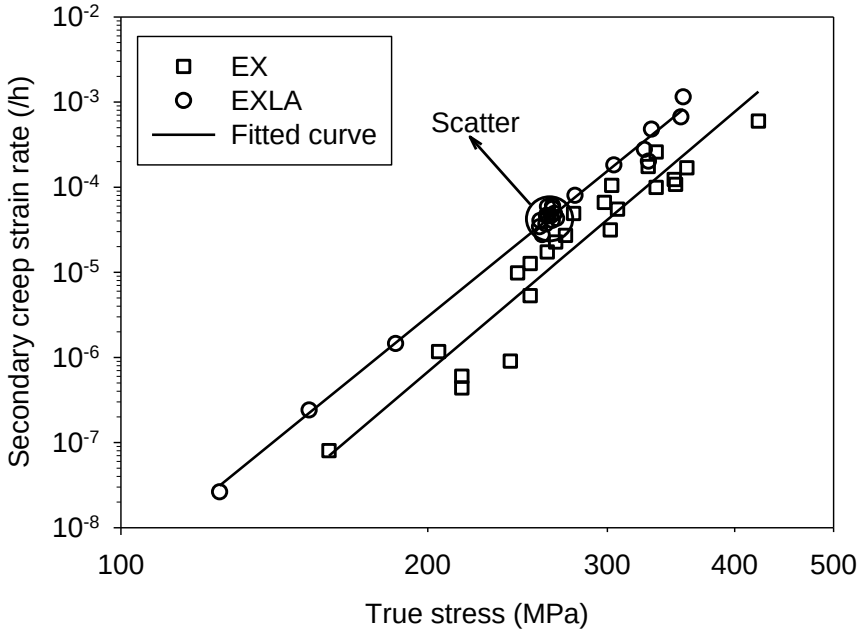

Figure 4. Secondary creep strain rates described by a stress dependent power law for Type 316H stainless in the ex-service laboratory aged (EXLA) and ex-service (EX) [18] condition.

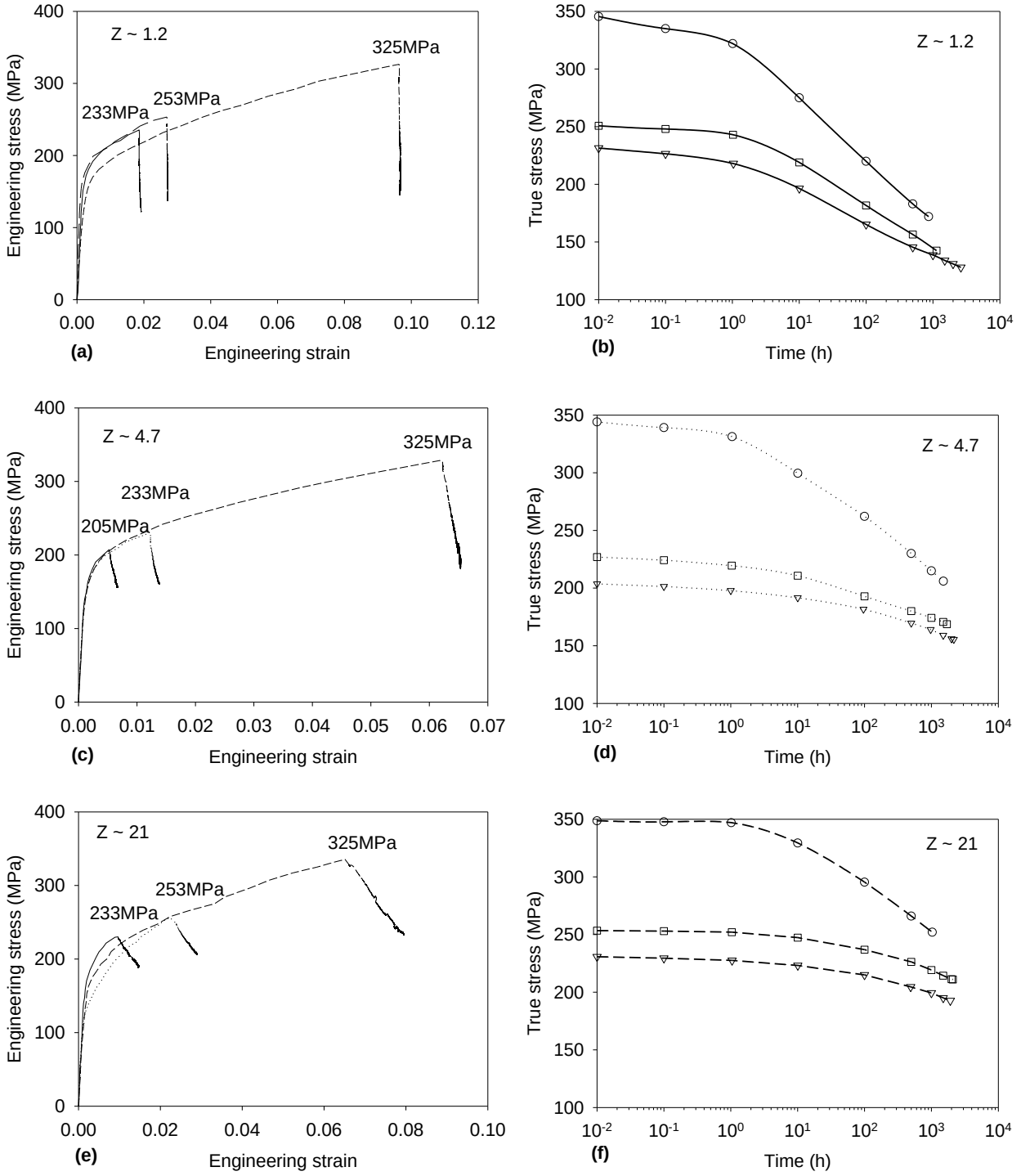

Figure 5. Comparison of stress relaxation with similar elastic follow-up factor but different initial applied stress. (a, c, e) The stress and strain trajectories for loading up and stress relaxation for similar elastic follow-up factors (1.2, 4.7 and 21) but different applied engineering stresses of 205 MPa, 230 MPa, 250 MPa and 350 MPa; (b, d, f) the corresponding true stress relaxation curves.

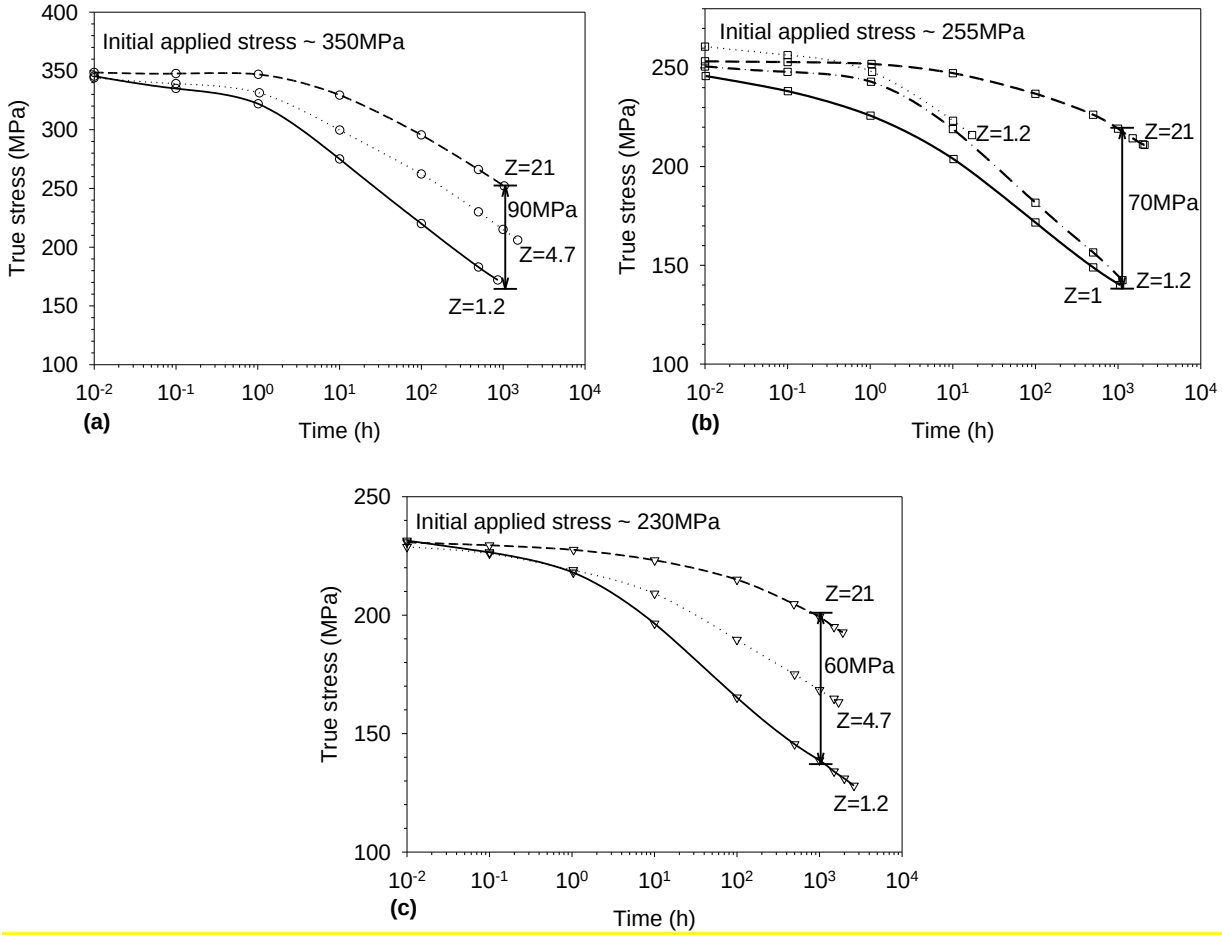

Figure 6. Stress relaxation with different elastic follow-up factors (Z) but similar levels of initial applied true stress (a) 350MPa, (b) 250MPa and (c) 230MPa.

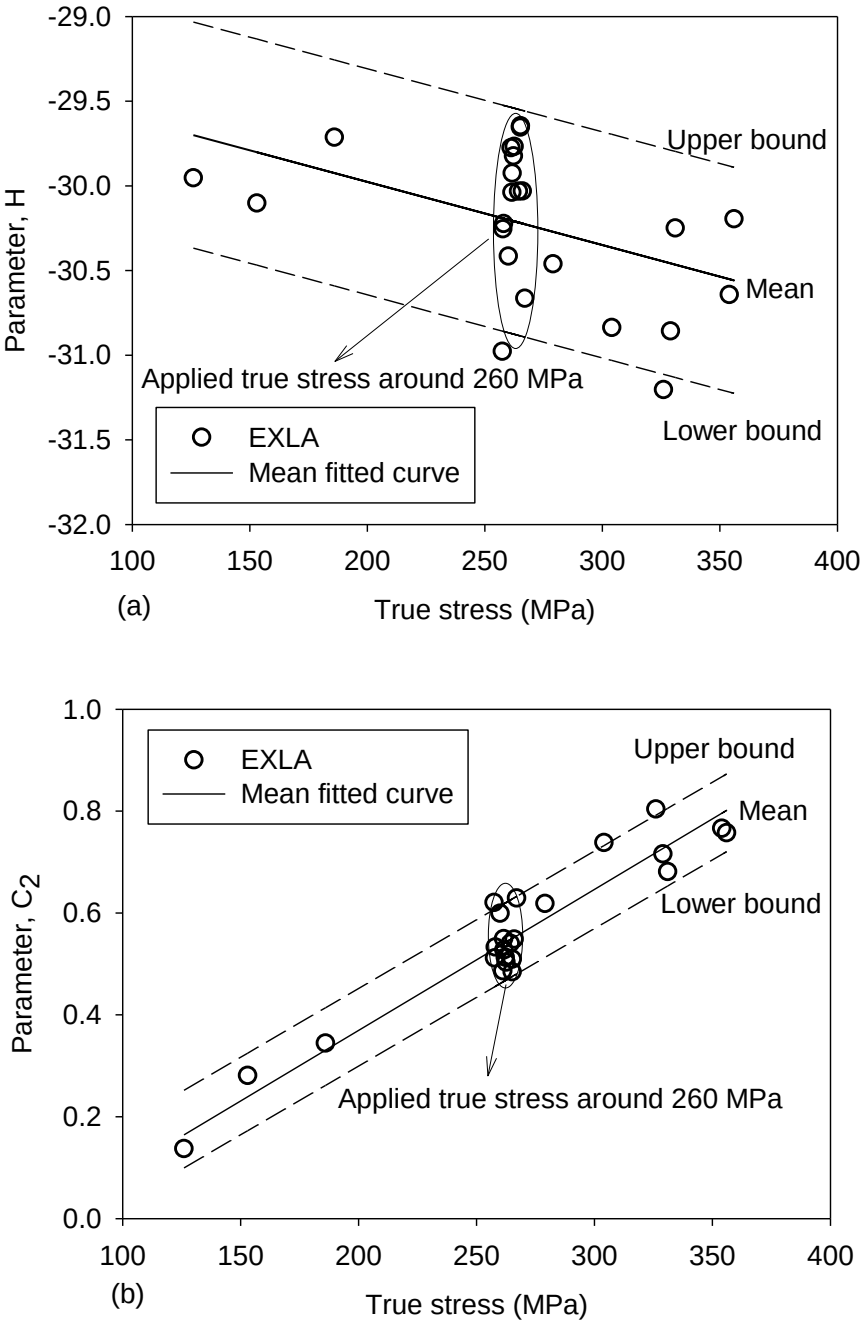

Figure 7. RCC-MR constants H and C_2 described by stress-dependent linear functions for Type 316H stainless steel in the ex-service laboratory aged (EXLA) condition at temperature 550 °C; (a) for primary creep constant H, (b) for primary creep constant C_2.

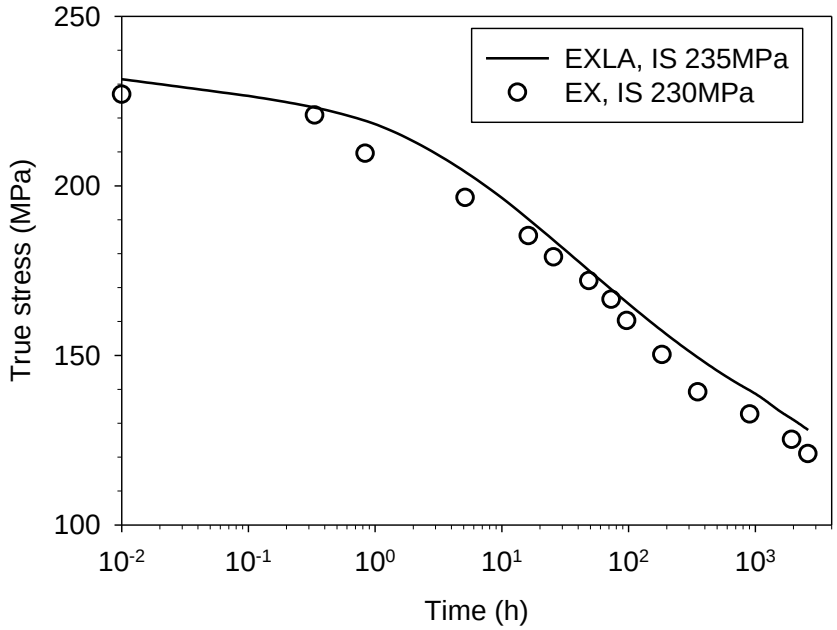

Figure 8. Creep stress relaxation of samples in EX [18] and EXLA conditions with similar initial applied stress of 230 MPa. IS represents initial applied stress.

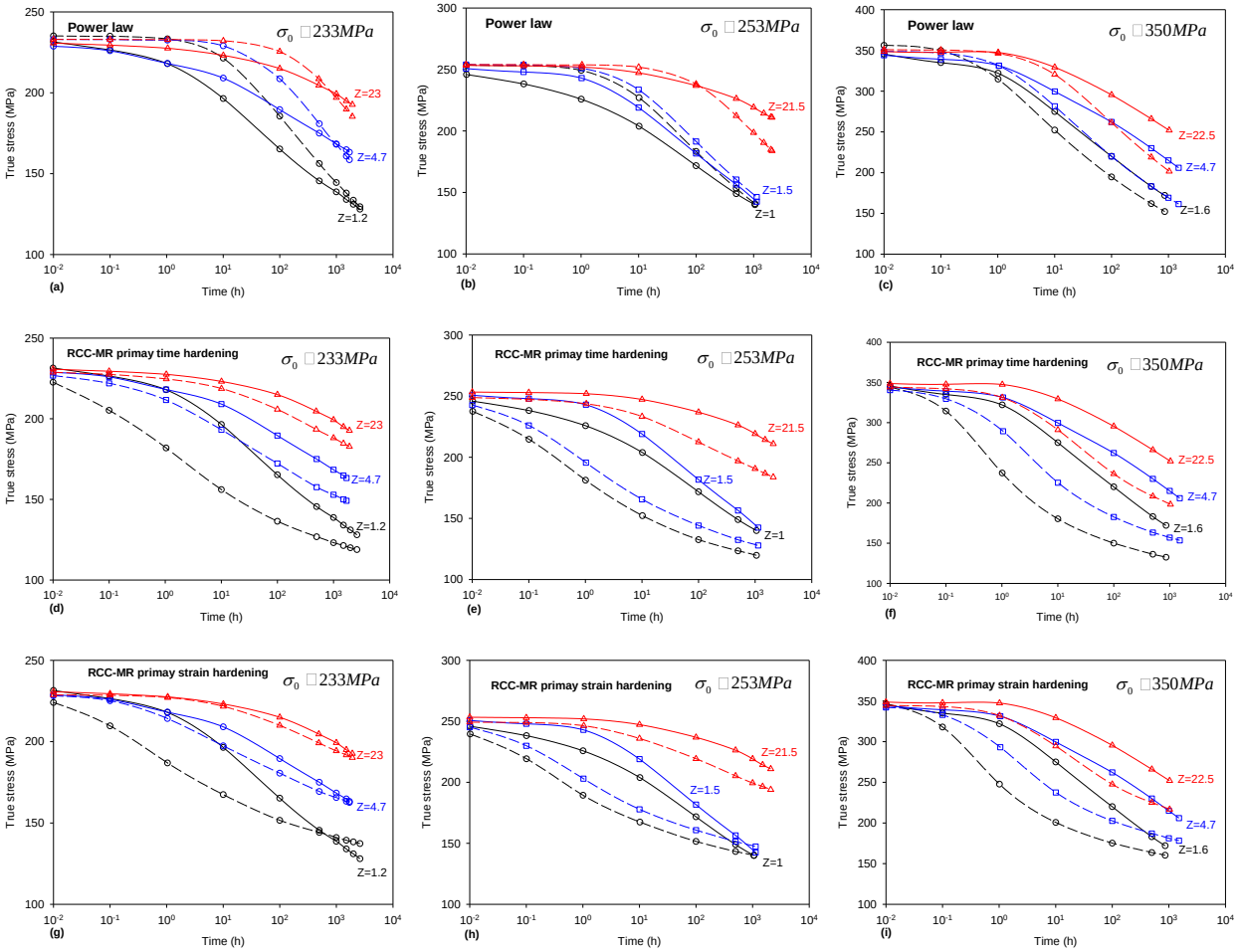

Figure 9. Prediction of creep stress relaxation with the effect of elastic follow-up by using (a, b, c) power law, (d, e, f) RCC-MR primary time hardening and (g, h, i) strain hardening with EXLA constants. Solid lines are experimental data while dashed lines are the corresponding predicted results.

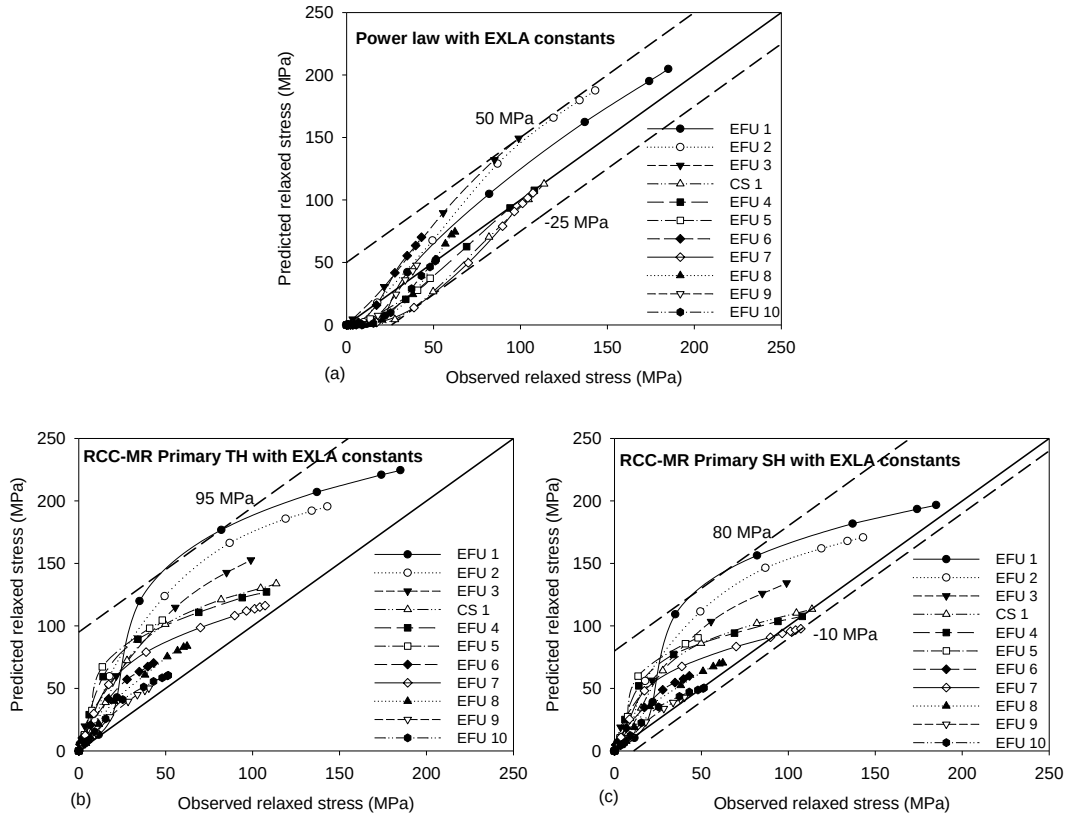

Figure 10. Predicted stress relaxation and elastic follow-up for Type 316H stainless steel in the ex-service laboratory aged (EXLA) condition using EXLA constants. Models using (a) power law and RCC-MR equations (b) Time Hardening (TH); and (c) Strain Hardening (SH) model.

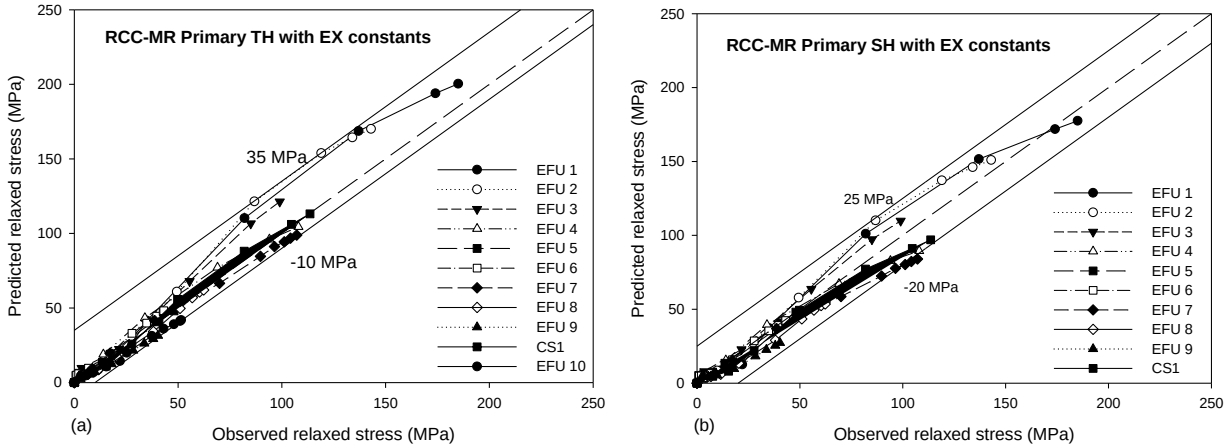

Figure 11. Predicted stress relaxation and elastic follow-up for Type 316H stainless steel in the ex-service laboratory aged (EXLA) condition by using EX constants. Models using RCC-MR primary equations (a) Time Hardening (TH) and (b) Strain Hardening (SH).

APPENDIX A: Calculation of elastic follow-up in a three-bar model

In a three-bar model, after loading up and during the creep under elastic follow-up control, the total strain in Bar 1 (specimen), Bar 2 and Bars 3 can be described as:

$$\left(\varepsilon_{1-e}+\varepsilon_{1-p}+\varepsilon_{1-c}\right)L_1+\left(\varepsilon_{2-e}+\varepsilon_{2-p}\right)L_2+\left(\varepsilon_{3-e}+\varepsilon_{3-p}\right)L_3=\delta \qquad \text{A1}$$

where ε_e, ε_p, ε_c, δ and L represent elastic strain, plastic strain, creep strain, total misfit and length of bars respectively. The subscripts 1, 2, 3 represent specimen, Bar 2 and Bars 3 respectively. It should be noted that the Eq. A1 assumes creep deformation only takes place in the specimen. The elastic and plastic deformation in bars and total misfit (δ) are constant during creep. Therefore, differentiating Equation A1 gives:

$$\dot{\varepsilon}_{1-e}L_1+\dot{\varepsilon}_{1-c}L_1+\dot{\varepsilon}_{2-e}L_2+\dot{\varepsilon}_{3-e}L_3=0 \qquad \text{A2}$$

where $\dot{\varepsilon}_{1-e}$ and $\dot{\varepsilon}_{1-c}$ are elastic and creep strain rate in the specimen, $\dot{\varepsilon}_{2-e}$ and $\dot{\varepsilon}_{3-e}$ are elastic strain rate in Bar 2 and Bars 3. Equilibrium conditions between these bars indicate that:

$$\dot{\varepsilon}_{2-e}=\frac{A_1E_1L_2}{A_2E_2}\dot{\varepsilon}_{1-e},\ \dot{\varepsilon}_{3-e}=\frac{A_1E_1L_3}{2A_3E_3}\dot{\varepsilon}_{1-e} \qquad \text{A3}$$

where A and E represent the area cross section and Young's modulus respectively. By substituting Eq. A3 into Eq. A2 we obtain:

$$\dot{\varepsilon}_{1-e}L_1\left(1+\frac{A_1E_1L_2}{A_2E_2L_1}+\frac{A_1E_1L_3}{2A_3E_3L_1}\right)+\dot{\varepsilon}_{1-c}L_1=0 \qquad \text{A4}$$

and rearranging:

$$\dot{\varepsilon}_{1-e}=-\frac{1}{Z}\dot{\varepsilon}_{1-c} \qquad \text{A5}$$

where Z is the elastic follow-up factor in the three bar system shown in Fig 1. For state 2 this gives:

$$Z=1+\frac{A_1E_1L_2}{A_2E_2L_1}+\frac{A_1E_1L_3}{2A_3E_3L_1}=1+1/\beta+1/\gamma=1+1/\alpha \qquad \text{A6}$$

where α, β and γ are the stiffness ratios between the specimen and the remaining parts of system. These are given by:

$$\alpha=K_T/K_1,\ \beta=K_2/K_1,\ \gamma=2K_3/K_1 \qquad \text{A7}$$

where K_1, K_2 and K_3 are the stiffness of the specimen, Bar 2 and Bars 3 respectively. K_T is the total stiffness of the system.

$$K_i = \frac{A_i E_i}{L_i}, i \in [1,\ 3] \quad \text{and} \quad K_T = 1 \Big/ \left(\frac{1}{K_2} + \frac{1}{2K_3} \right) \tag{A8}$$

where $i = 1,\ 2$ or 3 represents Bar 1, Bar 2 and Bars 3. A_i, E_i and L_i are the area cross section, Young's modulus and length of Bar 1, specimen and Bars 3 respectively.

The elastic strain in the specimen is given by:

$$\dot{\varepsilon}_{1\_e} = \frac{\dot{\sigma}_1}{E} \tag{A9}$$

Substituting Equation A9 to Equation A5 we get:

$$\dot{\sigma}_1 = -\frac{1}{Z} E_1 \dot{\varepsilon}_{1\_c} \tag{A10}$$

where $\dot{\sigma}_1$ is stress relaxation rate in the specimen, $\dot{\varepsilon}_{1\_c}$ is the creep strain rate in the specimen which can be described by any creep rate equation. According to Equation A10, the stress in the specimen will reduce as the elastic strain is replaced by creep strain. The total strain rate in the specimen during creep can be obtained by adding the elastic strain rate to the creep strain rate giving:

$$\dot{\varepsilon}_1 = \dot{\varepsilon}_{1\_e} + \dot{\varepsilon}_{1\_c} = (1 - Z) \frac{\dot{\sigma}_1}{E_1} \tag{A11}$$

Reference

[1] E. L. Robinson, "The resistance to relaxation of materials at high temperature," *Trans. ASME,* vol. 61, pp. 543-554, 1939.

[2] R. A. Ainsworth, "R5: Assessment procedure for the high temperature response of structures," *British Energy Generation Ltd,* vol. 3, 2003.

[3] RCC-MR. (1985). *Design and Construction Rules For Mechanical Components of FBR Nuclear Islands,Section 1, Sub-sections Z, Technical Appendix A3,AFCEN*.

[4] *ASME Boiler and Pressure Vessel Code, Section III-Rules for Construction of Nuclear Power Plant Components* vol. 2, 1992.

[5] P. J. Bouchard, P. J. Withers, S. A. McDonald, and R. K. Heenan, "Quantification of creep cavitation damage around a crack in a stainless steel pressure vessel," *Acta Materialia,* vol. 52, pp. 23-34, 2004.

[6] J. T. Boyle and K. Nakamura, "The assessment of elastic follow-up in high temperature piping systems—overall survey and theoretical aspects," *International Journal of Pressure Vessels and Piping,* vol. 29, pp. 167-194, 1987.

[7] K. Naoto, N. Takashi, I. Koji, and N. Hitoshi, "Advanced creep-fatigue evaluation rule for fast breeder reactor components: generalization of elastic follow-up model," *Nuclear Engineering and Design,* vol. 155, pp. 499-518, 1995.

[8] J. T. Boyle, "Elastic follow-up and the categorisation of secondary stress," *ASME PVP,* vol. 161, p. 7, 1989.

[9] N. Kasahara and M. Kikuchi, "Proposal of a strain concentration model of welded joints for creep-fatigue evaluation of welded structures," *JSME international journal. Series A, mechanics and material engineering,* vol. 40, pp. 247-254, 1997.

[10] K. Kobatake, H. Ohta, H. Ishiyama, T. Kaihara, and O. Ueno, "An alternate approach to creep-fatigue damage with elastic follow-up for high temperature structural design," *Journal of National Fisheries University,* vol. 48, pp. 25-39, 1999.

[11] J. T. Boyle, "Stress relaxation and elastic follow-up using a stress range-dependent constitutive model," *Proceedings of the Institution of Mechanical Engineers, Part C: Journal of Mechanical Engineering science,* vol. 226, pp. 1472-1483, 2012.

[12] Y. Q. Wang, D. J. Smith, and C. E. Truman, "Inelastic Deformation and Elastic Follow-Up," presented at the ASME 2013 Pressure Vessels and Piping Conference, 2013.

[13] K. Kobayashi, S. Abe, and T. Udoguchi, "Stress and strain behaviors under uniaxial elastic follow-up," *Bulletin of JSME,* vol. 29, pp. 3672-3678, 1986.

[14] N. Isobe, S. Sakurai, M. Yorikawa, K. Imou, and Y. and Takahashi, "Life prediction of 316FR stainless steel under creep–fatigue loading with elastic follow-up," *International journal of pressure vessels and piping,* vol. 77, pp. 817-823, 2000.

[15] D. J. Smith and A. M. Shirahatti, "The effects of long-range residual stress, elastic follow-up and applied load on creep crack incubation and material toughness," *The Journal of Strain Analysis for Engineering Design,* p. 0309324715595315, 2015.

[16] M. Yamashita and Y. Wada, "The stress-relaxation behavior of type 304 stainless steel," *International Journal of Pressure Vessels and Piping,* vol. 42, pp. 203-216, 1990.

[17] K. Kobayashi, Y. Saitoh, and T. Udoguchi, "Estimation of elastic follow-up behavior on 18Cr-8Ni steel using simplified inelastic analysis," *Journal of Pressure Vessel Technology,* vol. 116, pp. 136-140, 1994.

[18] Y. Q. Wang, M. W. Spindler, C. E. Truman, and D. J. Smith, "Critical analysis of the prediction of stress relaxation from forward creep of Type 316H austenitic stainless steel," *Materials & Design,* vol. 95, pp. 656-668, 2016.

[19] E. Krempl, "Relaxation behavior and modeling," *International journal of Plasticity,* vol. 17, pp. 1419-1436, 2001.

[20] B. Chen, J. N. Hu, Y. Q. Wang, S. Y. Zhang, S. Van Petegem, A. C. F. Cocks, *et al.*, "Role of the misfit stress between grains in the Bauschinger effect for a polycrystalline material," *Acta Materialia,* vol. 85, pp. 229-242, 2015.

[21] T. D. Joseph, D. McLennon, M. W. Spindler, C. E. Truman, and D. J. Smith, "The effect of prior cyclic loading variables on the creep behaviour of ex-service Type 316H stainless steel," *Materials at High Temperatures,* vol. 30, pp. 156-160, 2013.

[22] B. Chen, J. N. Hu, P. E. J. Flewitt, D. J. Smith, A. C. F. Cocks, and S. Y. Zhang, "Quantifying internal stress and internal resistance associated with thermal ageing and creep in a polycrystalline material," *Acta Materialia,* vol. 67, pp. 207-219, 2014.

[23] "ASTM Standard E8-96a, Standard Test Methods for Tension Testing of Metallic Materials," *Annual Book*

of ASTM Standards, vol. 03.01. American Society for Testing and Materials, West Conshohocken, PA., pp. 57-72, 2001.

[24] "British Standards Institute, Metallic Materials – Uniaxial Creep Testing in Tension – Method of Test," *BS EN 10291:2000, London*, 2000.

[25] Y. Q. Wang, A. M. Shirahatti, C. E. Truman, and D. J. Smith, "Prediction of creep crack initiation under the interaction between long range residual stress and applied load," presented at the ICF 13, Beijing, China, 2013.

[26] Y. Q. Wang, "Design, development and experiments to investigate the effect of elastic follow-up on creep stress relaxation in austenitic steels," PhD thesis submitted to Department of Mechanical Engineering, University of Bristol, UK, 2015.

[27] G. Webster, C. Davies, and K. Nikbin, "Assessment of creep crack growth due to stress relief," *International Journal of Solids and Structures*, vol. 47, pp. 881-886, 2010.

[28] B. R. Hunt, R. L. Lipsman, and J. M. Rosenberg, *A guide to MATLAB: for beginners and experienced users*: Cambridge University Press, 2014.

[29] J. H. Gittus, "Theoretical scatter of creep-relaxation measurements versus the scatter in constant-load creep data," *Philosophical Magazine*, vol. 20, pp. 1189-1193, 1969.

[30] A. Mehmanparast, C. M. Davies, D. W. Dean, and K. Nikbin, "Effects of plastic pre-straining level on the creep deformation, crack initiation and growth behaviour of 316H stainless steel," *International journal of pressure vessels and piping*, vol. 141, pp. 1-10, 2016.

[31] J. H. Gittus, "Theoretical scatter of creep-relaxation measurements versus the scatter in constant-load creep data," *Philosophical Magazine*, vol. 20, pp. 1189-1193, 1969.

[32] M. Rieth, A. Falkenstein, P. Graf, S. Heger, U. Jantsch, M. Klimiankow, *et al.*, "Creep of the austenitic steel AISI 316L(N): experiments and models," *Tech. rep., Forschungszentrum Karlsruhe, FZKA 7065, Karlsruhe*, 2004.

[33] "National Institute of Materials Science N. Micrographs and Microstructural Characterisitcs of Crept Specimens of 18Cr-12Ni-Mo Stainless steel for Boiler and Heat exchanger seamless tubes (SUS 316H TB)," 2003.

[34] J. N. Hu, "A theoretical study of creep deformation mechanisms of type 316H stainless steel at elevated temperatures, " Department of Engineering Science, Ph.D, University of Oxford, Oxford; 2015.

[35] M. R. Daymond and P. J. Bouchard, "Elastoplastic deformation of 316 stainless steel under tensile loading at elevated temperatures," *Metallurgical and Materials Transactions A*, vol. 37, pp. 1863-1873, 2006.

[36] R. Lin Peng, M. Odén, Y. Wang, and S. Johansson, "Intergranular strains and plastic deformation of an austenitic stainless steel," *Materials Science and Engineering: A*, vol. 334, pp. 215-222, 2002.

[37] B. Clausen, T. Lorentzen, and T. Leffers, "Self-consistent modelling of the plastic deformation of fcc polycrystals and its implications for diffraction measurements of internal stresses," *Acta Materialia*, vol. 46, pp. 3087-3098, 1998.

[38] A. A. Mamun, R. J. Moat, J. Kelleher, and P. J. Bouchard, "Generation of intergranular strains during high temperature creep fatigue loading of 316H stainless steel," *Materials at High Temperatures*, vol. 31, pp. 378-382, 2014.

[39] E. Salvati and A. M. Korsunsky, "An analysis of macro-and micro-scale residual stresses of Type I, II and III using FIB-DIC micro-ring-core milling and crystal plasticity FE modelling," *International Journal of Plasticity*, vol. 98, pp. 123-138, 2017.

[40] A. Rao, P. J. Bouchard, S. M. Northover, and M. E. Fitzpatrick, "Anelasticity in austenitic stainless steel," *Acta Materialia*, vol. 60, pp. 6851-6861, 2012.

[41] B. Chen, P. E. J. Flewitt, A. C. F. Cocks, and D. J. Smith, "A review of the changes of internal state related to high temperature creep of polycrystalline metals and alloys," *International Materials Reviews*, vol. 60, pp. 1-29, 2014.

[42] J. N. Hu and A. C. F. Cocks, "Effect of creep on the Bauschinger effect in a polycrystalline austenitic stainless steel," *Scripta Materialia*, vol. 128, pp. 100-104, 2017.

[43] J. N. Hu, B. Chen, D. J. Smith, P. E. J. Flewitt, and A. C. F. Cocks, "On the evaluation of the Bauschinger effect in an austenitic stainless steel—The role of multi-scale residual stresses," *International Journal of Plasticity*, Vol. 84, pp. 203-223, 2016.

[44] Y. Wang, S. Hossain, S. Kabra, S. Zhang, D. Smith, and C. Truman, "Effect of boundary conditions on the evolution of lattice strains in a polycrystalline austenitic stainless steel," *Journal of Materials Science*, vol. 52, pp. 7929-7936, 2017.

[45] Y. Wang, S. Kabra, S. Zhang, D. Smith, and C. Truman, "An in situ thermo-mechanical rig for lattice strain

measurement during creep using neutron diffraction," *Review of Scientific Instruments*, Under reivew, 2017.
[46] T. L. Burnett, R. Geurts, H. Jazaeri, S. M. Northover, S. A. McDonald, S. J. Haigh, *et al.*, "Multiscale 3D analysis of creep cavities in AISI type 316 stainless steel," *Materials Science and Technology,* vol. 31, pp. 522-534, 2015.
[47] A. D. Warren, I. J. Griffiths, R. L. Harniman, P. E. J. Flewitt, and T. B. Scott, "The role of ferrite in Type 316H austenitic stainless steels on the susceptibility to creep cavitation," *Materials Science and Engineering: A*, vol. 635, pp. 59-69, 2015.
[48] A. I. Martinez-Ubeda, A. D. Warren, I. Griffiths, and P. E. J. Flewitt, "The Role of Prior Fabrication and in Service Thermal Ageing on the Creep Life of AISI Type 316 Stainless Steel Components," in *Key Engineering Materials*, 2016, pp. 1-4.
[49] J. Intrater and E. S. Machlin, "Grain boundary sliding and intercrystalline cracking," *Acta metallurgica*, vol. 7, pp. 140-143, 1959.
[50] B. Senior, "Effect of phase transformations on the creep rupture properties of two type 316 weld metals," *Journal of materials science*, vol. 25, pp. 45-53, 1990.
[51] B. F. Dyson, "Continuous cavity nucleation and creep fracture," *Scripta Metallurgica*, vol. 17, pp. 31-37, 1983.
[52] M. Kassner and T. Hayes, "Creep cavitation in metals," *International Journal of Plasticity,* vol. 19, pp. 1715-1748, 2003.
[53] F. D. Fischer, J. Svoboda, T. Antretter, and E. Kozeschnik, "Relaxation of a precipitate misfit stress state by creep in the matrix," *International Journal of Plasticity,* vol. 64, pp. 164-176, 2015.
[54] J. Svoboda, F. Fischer, H. Riedel, and E. Kozeschnik, "Precipitate growth in multi-component systems with stress relaxation by diffusion and creep," *International Journal of Plasticity,* vol. 82, pp. 112-126, 2016.
[55] Y. F. Yin, Faulkner, R.G, "Creep life predictions in 9% Cr ferritic steels In: Proceeding of International Conference on New Developments on Metallurgy and Applications of High Strength Steels (TMS)," Buenos Aires, Argentina, pp. 283–296, 2008.
[56] J. Cadek, "Creep in metallic materials," 1988.
[57] M. Basirat, T. Shrestha, G. Potirniche, I. Charit, and K. Rink, "A study of the creep behavior of modified 9Cr–1Mo steel using continuum-damage modeling," *International Journal of Plasticity,* vol. 37, pp. 95-107, 2012.
[58] B. Chen, J. N. Hu, P. E. J. Flewitt, A. C. F. Cocks, R. A. Ainsworth, D. J. Smith, *et al.*, "Effect of thermal ageing on creep and oxidation behaviour of Type 316H stainless steel," *Materials at High Temperatures*, vol. 32, pp. 592-606, 2015.
[59] B. Chen, J. N. Hu, Y. Q. Wang, S. Kabra, A. C. F. Cocks, D. J. Smith, *et al.*, "Internal strains between grains during creep deformation of an austenitic stainless steel," *Journal of Materials Science*, vol. 50, pp. 5809-5816, 2015.